JOURNAL OF SOLID STATE CHEMISTRY **108**, 177–183 (1994)

The Mixed Valent Molybdenum Monophosphate $RbMo_2P_2O_{10} \cdot (1 - x)H_2O$: An Intersecting Tunnel Structure Isotypic with Leucophosphite

A. Leclaire, M. M. Borel, A. Grandin, and B. Raveau

Laboratoire CRISMAT, URA 1318 associé au CNRS, ISMRA Université de Caen, Boulevard du Maréchal Juin 14050 Caen Cedex, France

Received December 7, 1992; in revised form May 7, 1993; accepted May 13, 1993

A new molybdenum monophosphate $RbMo_2P_2O_{10} \cdot (1 - x)H_2O$, with the mixed valence Mo(V)–Mo(IV) has been synthesized by conventional techniques. Its structure has been solved from single crystal X-ray diffraction in the space group $P2_1/c$ with $a = 9.789(1)$ Å, $b = 9.752(1)$ Å, $c = 12.347(1)$ Å, $\beta = 128.81(1)°$. This compound, isotypic with $NH_4Mo_2P_2O_{10} \cdot H_2O$ described by King *et al.*, *J. Solid State Chem.* 92, 1 (1991), exhibits the leucophosphite structure. A new description of this open framework, involving $[MoPO_8]_\infty$ chains and $Mo_2P_2O_{10}$ units built up of two edge-sharing MoO_6 octahedra bridged by two PO_4 tetrahedra, is proposed. The Rb phosphate differs from the NH_4 phase by the distribution of Rb^+ cations which partially occupy three kinds of sites, whereas one observes only one sort of site, fully occupied, in the ammonium phase. The possibility of a large stoichiometry deviation in the interpolated cation is considered. © 1994 Academic Press, Inc.

INTRODUCTION

The studies of the molybdenum phosphates performed these last ten years have allowed a large variety of compounds, characterized by different original mixed frameworks and various oxidation states of molybdenum to be isolated. In spite of the great adaptability of MoO_6 octahedra to PO_4 tetrahedra, very few phosphates involving a mixed valence of molybdenum were synthesized (1–12). Among them the phosphate $NH_4Mo_2P_2O_{10} \cdot H_2O$ isolated recently by King *et al.* (11), represents the only phosphate with the mixed valence Mo(IV)–Mo(V). This compound is of great interest for its possible use as a precursor to generate catalysts by combining the low oxidation state of molybdenum and the microporous character of the structure; indeed the latter was shown by the authors to be isotypic with the mineral leucophosphite. However, such an open framework, seems to be difficult to obtain since it could only be prepared by hydrothermal synthesis at very high pressures in the form of very tiny crystals (11). In order to reach a better understanding of the stability of this structure, we have tried to introduce a larger cation than ammonium, like rubidium. The present paper reports on the crystal structure of the isotypic monophosphate $RbMo_2P_2O_{10} \cdot (1 - x)H_2O$ prepared by a conventional technique.

SYNTHESIS

Single crystals of this new phosphate were grown from a mixture of nominal composition "$RbMo_2P_2O_{10}$." First $H(NH_4)_2PO_4$, Rb_2CO_3 and MoO_3 were mixed in an agate mortar in adequate ratios according to the composition "$RbMo_{1.5}P_2O_{10}$" and heated at 600 K in a platinum crucible to decompose the ammonium phosphate and carbonate. In a second step the resulting mixture was then added to the required amount of molybdenum (0.5 mole), placed in an alumina tube and sealed in an evacuated silica ampoule, then heated for one day at 1073 K and cooled at 1.3 K per hour down to 873 K. The sample was finally quenched to room temperature.

Two sorts of crystals were extracted from the resulting product, with a yellow and black color respectively. The yellow crystals were identified as β-$RbMo_2P_3O_{13}$ previously synthesized (13). The microprobe analysis of the black crystals confirmed the composition $RbMo_2P_2O_{10} \cdot (1 - x)H_2O$ ($x \approx 0.10$) deduced from the structure determination.

Many attempts to prepare large amounts of this new phase in the form of powder always led to a mixture with β-$RbMo_2P_3O_{13}$. Thus, black crystals were picked out with tweezers, using a binocular in order to perform further characterizations. The crystals were then crushed, leading to a red brown powder which was studied by TGA, infrared spectroscopy and X-ray powder diffraction.

The infrared spectra registered with a Nicolet 60 SX spectrometer indicated the presence of water. The thermogravimetric analysis confirmed this feature. A weight loss of 2.98% at 423 K was observed, consistent with

0022-4596/94 $6.00

TABLE 1
Intereticular Distances $RbMo_2P_2O_{10} \cdot (1 - x)H_2O$ ($x = 0.1$) in the $P2_1/n$ Space Group

h	*k*	*l*	d_{calc}	d_{obs}	*I*	*h*	*k*	*l*	d_{calc}	d_{obs}	*I*
1	0	0	7.628	7.593	35	2	3	$\bar{3}$	2.515	2.513	1
0	1	1	6.849	6.831	100	3	1	0	2.460	2.459	4
1	1	$\bar{1}$	6.831			0	0	4	2.405	2.403	2
1	0	$\bar{2}$	6.173	6.163	2	0	4	1	2.363	2.362	1
1	1	0	6.008	5.991	12	3	1	$\bar{5}$	2.363		
2	0	$\bar{2}$	4.786	4.769	3	1	4	$\bar{1}$	2.363		
0	2	1	4.349	4.347	3	4	1	$\bar{4}$	2.324	2.322	2
1	2	$\bar{1}$	4.345			1	4	0	2.322		
2	1	$\bar{2}$	4.297	4.291	3	3	3	$\bar{3}$	2.277	2.277	7
2	1	$\bar{1}$	4.229	4.225	5	3	2	$\bar{5}$	2.179	2.177	7
1	2	0	4.108	4.104	4	4	2	$\bar{2}$	2.114	2.112	1
2	0	0	3.814	3.809	5	4	1	$\bar{1}$	2.094	2.094	2
1	1	$\bar{3}$	3.684	3.689	1	2	4	$\bar{3}$	2.079	2.078	1
2	1	0	3.552	3.547	11	3	3	0	2.003	2.003	3
0	2	2	3.416	3.413	21	2	0	$\bar{6}$	1.989	1.989	2
1	2	1	3.388	3.387	4	1	3	3	1.960	1.961	1
0	3	1	3.079	3.079	27	2	3	$\bar{5}$	1.951	1.951	1
1	3	$\bar{1}$	3.078			0	4	3	1.941	1.941	3
2	2	$\bar{3}$	3.078			4	0	0	1.907	1.906	3
3	1	$\bar{3}$	3.033	3.030	1	3	4	1	1.883	1.883	1
2	2	0	3.004	3.002	29	3	4	$\bar{4}$	1.854	1.855	1
2	1	$\bar{4}$	2.943	2.939	4	4	2	$\bar{6}$	1.838	1.837	2
3	1	$\bar{1}$	2.831	2.827	11	1	3	$\bar{5}$	1.836		
3	2	$\bar{2}$	2.697	2.694	11	1	5	1	1.802	1.803	6
0	3	2	2.693			3	3	1	1.792	1.790	3
2	3	$\bar{1}$	2.672	2.672	10	0	2	5	1.790		
3	2	$\bar{3}$	2.670			3	4	0	1.760	1.759	1
2	2	$\bar{4}$	2.608	2.615	3	1	4	3	1.731	1.731	1
3	0	0	2.542	2.539	18	3	2	2	1.709	1.709	6

TABLE 3
Summary of Data Intensity, Measurements and Structure Refinement Parameters for $RbMo_2P_2O_{10} \cdot (1 - x)H_2O$ ($x = 0.1$)

1. Crystal data	
Space group	$P2_1/c$
Cell dimensions	$a = 9.789(1)$ Å $b = 9.752(1)$ $c = 12.347(1)$ $\beta = 128.81(1)°$
volume	$V = 918.5(3)$ Å^3
Z	4
ρ_{calc} (g cm^{-3})	3.74
ρ_{exp} (g cm^{-3})	3.79
2. Intensity measurements	
λ(Mo*K*α)	0.71073 Å
Scan mode	$\omega-\frac{2}{3}\theta$
Scan width (°)	$1.23 + 0.35 \tan\theta$
Slit aperture (mm)	$1.24 + \tan\theta$
Max θ(°)	45
Standard reflections	3 every 3000 sec (no decay)
Reflections with $I > 3\sigma$	1372
μ(mm^{-1})	8.19
3. Structure solution and refinement	
Parameters refined	96
Agreement factors	$R = 0.043$, $R_w = 0.049$
Weighting scheme	$w = f(\sin\theta/\lambda)$
Δ/σ_{max}	0.01

the formula $RbMo_2P_2O_{10} \cdot 0.9H_2O$ deduced from the single crystal X-ray study (3.10%) was observed. Moreover, the zeolithic character of the structure was evident: the structure was maintained up to 423 K and reabsorbed atmospheric water at room temperature.

The powder X-ray diffraction pattern of this phosphate was indexed in a monoclinic cell (Table 1) in agreement with the parameters obtained from the single crystal X-ray study (Table 2).

STRUCTURE DETERMINATION

The poor quality of the crystals forced us to test many of them before finding a crystal with well resolved reflections. A black crystal with dimensions 0.039 × 0.039 × 0.039 mm^3 was selected for the structure determination. The cell parameters were determined and refined by diffractometric techniques at 294 K with a least-squares refinement based upon 25 reflections with $18° \leq \theta \leq 25°$.

TABLE 2
Crystallographic Parameters

	a(Å)	*b*(Å)	*c*(Å)	β°	*V*(Å^3)
$RbMo_2P_2O_{10} \cdot 0.9H_2O$	9.786(3)	9.762(21)	9.838(2)	102.04(2)	919(1)
$NH_4Mo_2P_2O_{10} \cdot H_2O$	9.780(10)	9.681(5)	9.884(8)	102.17(8)	915(1)

The powder and single crystal X-ray diffraction investigation shows a monoclinic cell, with the space group $P2_1/n$ similar to that of $NH_4Mo_2P_2O_{10} \cdot H_2O$ (Table 2). The structure resolution in this space group, led us to a permutation of the *a* and *c* axis with respect to the ammonium phosphate. For this reason we prefered to solve the structure in the $P2_1/c$ group with the cell parameters given in Table 3. The reflections were corrected for Lorentz, polarization, and secondary extinction effects. No absorption corrections were performed. The structure was solved by the heavy atom method. The refinement of the coordinates and anisotropic thermal factors for Mo(1), Mo(2), Rb(1), Rb(2), and OH_2 and isotropic thermal factors for the other atoms led to $R = 0.043$ and $R_w = 0.049$ and to the atomic parameters of Table 4.

DESCRIPTION OF THE STRUCTURE AND DISCUSSION

The $[Mo_2P_2O_{10}]_\infty$ host lattice of $RbMo_2P_2O_{10} \cdot 0.9H_2O$ is very similar to that of $NH_4Mo_2P_2O_{10} \cdot H_2O$. The projec-

TABLE 4

Positional Parameters and Their Estimated Standard Deviations

Atom	x	y	z	B (Å^2)
Mo(1)	0.24602(9)	0.1966(1)	0.16663(8)	0.28(1)
Mo(2)	−0.01442(9)	0.0319(1)	0.39763(7)	0.21(1)
P(1)	0.1526(3)	0.3084(3)	0.3593(2)	0.03(4)*
P(2)	0.6313(3)	0.0142(3)	0.3403(2)	0.04(4)*
Rb(1)	0.6475(2)	0.3215(2)	0.1264(1)	2.59(3)
Rb(2)	0.662(2)	0.182(2)	0.038(1)	3.4(4)
Rb(3)	0.500	0.000	0.000	3.1(9)*
O(1)	0.114(1)	0.066(1)	0.1273(8)	1.9(2)*
O(2)	0.2818(8)	0.2524(9)	0.3394(7)	1.0(1)*
O(3)	0.2639(8)	0.1608(9)	0.0150(7)	1.1(1)*
O(4)	0.0647(8)	0.3501(8)	0.0589(6)	0.9(1)*
O(5)	0.4759(9)	0.0986(9)	0.3000(7)	1.3(1)*
O(6)	0.4251(8)	0.3709(9)	0.2165(7)	1.1(1)*
O(7)	0.0063(8)	0.2066(9)	0.3144(7)	1.2(1)*
O(8)	−0.0693(8)	−0.0610(9)	0.2254(7)	1.3(1)*
O(9)	0.2391(8)	−0.0087(8)	0.4971(6)	1.0(1)*
O(10)	−0.2676(8)	0.0822(9)	0.2943(6)	1.0(1)*
OH2	0.753(1)	0.338(1)	0.488(1)	3.0(3)

Note. Starred atoms were refined isotropically. Anisotropically refined atoms are given in the form of the isotropic equivalent displacement parameter defined as:

$$B = (\tfrac{4}{3}) \Sigma_i \Sigma_j \beta_{ij} \mathbf{a}_i \cdot \mathbf{a}_j.$$

tions of the structure along [010] (Fig. 1a), [001] (Fig. 1b), and [100] (Fig. 1c) show large tunnels running along these directions, and emphasize the microporous character of this structure.

On the projection of the structure perpendicular to (100) (Fig. 2) one recognizes the Mo_4O_{20} units bridged by PO_4 tetrahedra (Fig. 3) previously described by King *et al.* (11).

In fact this view of the structure allows a single description of this structure to be proposed. It involves $[MoPO_8]_\infty$ chains in which one MoO_6 octahedron alternates with one PO_4 tetrahedron along **c**, already encountered in many phosphates of transition elements (14), and $Mo_2P_2O_{14}$ structural units (Fig. 4) built up from two edge-sharing MoO_6 octahedra bridged by two PO_4 tetrahedra. Thus the $[Mo_2P_2O_{10}]_\infty$ framework can be described from the assemblage of $[MoPO_8]_\infty$ chains through $Mo_2P_2O_{14}$ units along two directions, $[2\bar{1}1]$ and [211] as shown in Fig. 2; note that the edge-sharing MoO_6 octahedra of the $Mo_2P_2O_{14}$ units share their two common apices with two octahedra of two $[MoPO_8]_\infty$ chains so that the corresponding oxygen atoms are triply bonded.

The PO_4 tetrahedra, which share their four apices with MoO_6 octahedra have a very similar geometry to that observed in $NH_4Mo_2P_2O_{10} \cdot H_2O$ (Table 5). Note that the P(1) tetrahedra, with O–O distances ranging from 2.43 to 2.55 Å are more distorted than the P(2) tetrahedra (O–O distances ranging from 2.47 to 2.56 Å), though they exhibit more homogeneous distances (1.52–1.53 Å) for P(1) against (1.50–1.56 Å for P(2)). This difference comes from the fact two oxygen atoms of P(2) are more strongly linked to rubidium than the other ones.

The Mo(2) octahedra which form the $Mo_2P_2O_{14}$ units are characterized by rather homogeneous Mo–O distances ranging from 1.99 to 2.06 Å (Table 5). The remarkable structural feature deals with the very short Mo(2)–Mo(2) distances of 2.442 Å, between the Mo atoms of the two edge-sharing octahedra. This distance is close to that observed for the ammonium phosphate by King *et al.* (11) (2.453 Å) and described by these authors as a Mo–Mo double bond. The valence calculations according to the Brown and Altermatt model (15), confirms that molybdenum in these edge-sharing octahedra is tetravalent (3.99). The Mo(1) octahedra which form the $[MoPO_8]_\infty$ chains are linked to four PO_4 tetrahedra, and share one apex triply bonded oxygen with the two edge-sharing Mo(2) octahedra, their sixth corner being free. The valence calculations show that this molybdenum atom is pentavalent (5.01). Indeed the geometry of these octahedra (Table 5) is characteristic of Mo(V), with an abnormally short Mo–O bond of 1.65 Å characteristic of the molybdenyl ion, the longer Mo–O distance of 2.23 Å corresponding to the opposing bond.

The main difference between the rubidium and the ammonium phosphates deals with the distribution of cations and water molecules in the tunnels. The water molecules are located in the tunnels running along **c**, in the same position as in the ammonium monophosphate. However only 90% of the sites are occupied in the rubidium phosphate, whereas these sites are fully occupied in the ammonium phosphate. This is due to a different distribution of the rubidium cations, which do not occupy only one site contrary to ammonium, but are distributed over three sites labelled Rb(1), Rb(2), and Rb(3). The Rb(1) sites which are located at the intersection of the [010] and [001] tunnels, correspond to the NH_4^+ positions; 85% of the rubidium cations are located in these sites, and are surrounded by 11 oxygen cations with distances ranging from 2.876 to 3.49 Å, one of the oxygens belonging to the H_2O molecule. Note that the polyhedron can be described as a distorted Archimedian antiprism with one square face and two opposite triangular capped faces. The Rb(2) sites, which were not occupied in the ammonium phase, are 10% occupied in the rubidium phosphate. In these sites which are located at the intersection of the [010] and [001] tunnels, rubidium exhibits a sevenfold coordination, with Rb–O distances ranging from 2.94 to 3.27 Å (Table 5). Note that the RbO_7 polyhedron can be described as a pyramid with two opposite triangular capped faces.

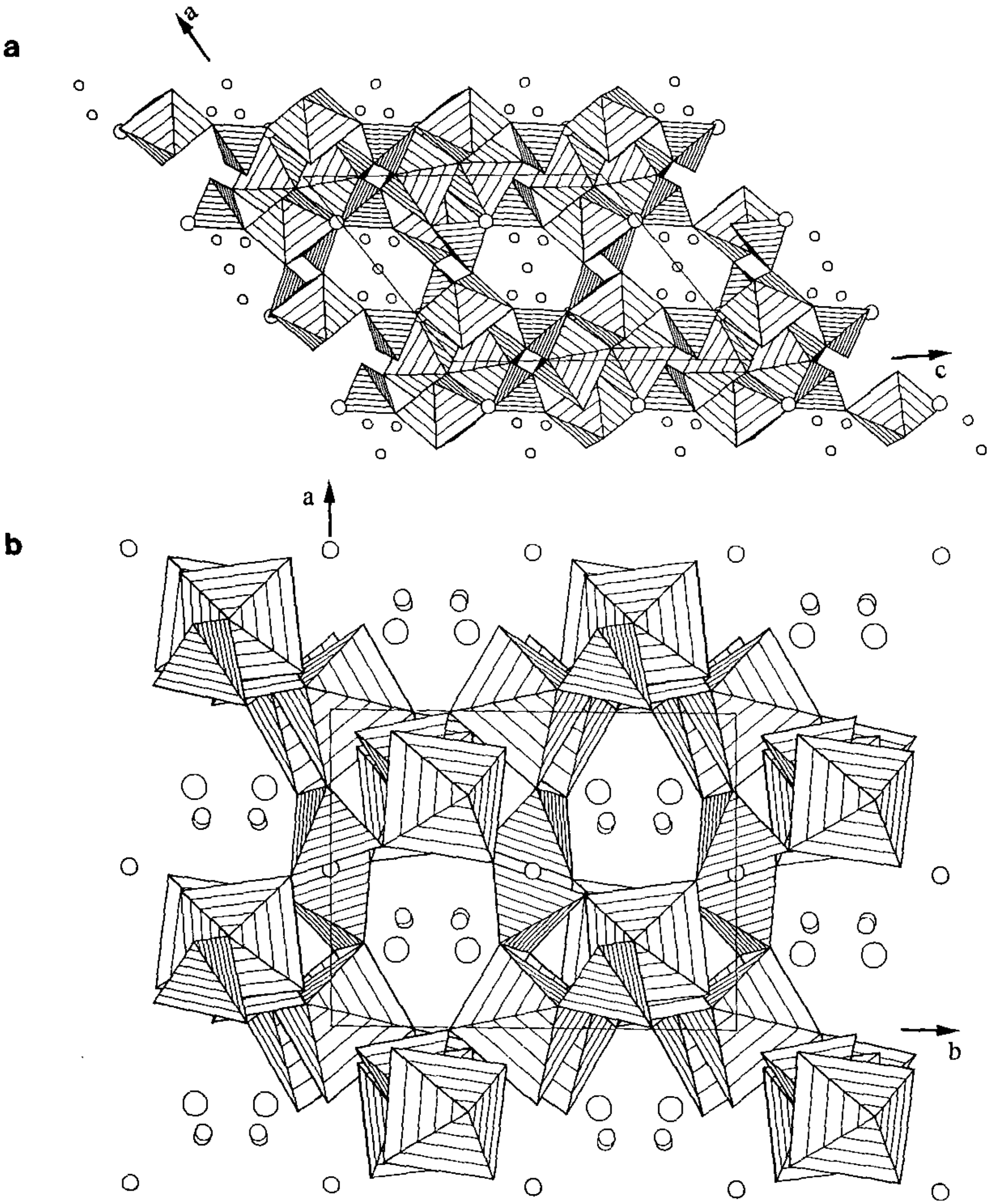

FIG. 1. Projection of the structure of $RbMo_2P_2O_{10} \cdot 0.9H_2O$. (a) along **b**, (b) along **c**, (c) along **a**, showing the tunnels.

It is also remarkable that this site is located very near the H_2O position, so that both sites cannot be occupied simultaneously; for this reason 10% of the H_2O sites are unoccupied in the rubidium monophosphate. The Rb(3) site, which is located in the center of symmetry at the intersection of the [010] and [100] tunnels, is 5% occupied. In this site, rubidium is surrounded by 12 oxygen atoms with Rb–O distances ranging from 2.89 to 3.34 Å; two of these oxygen atoms, located at 3.02 Å, belong to the H_2O molecules. This RbO_{12} polyhedron can be described as a distorted dicapped pentagonal antiprism.

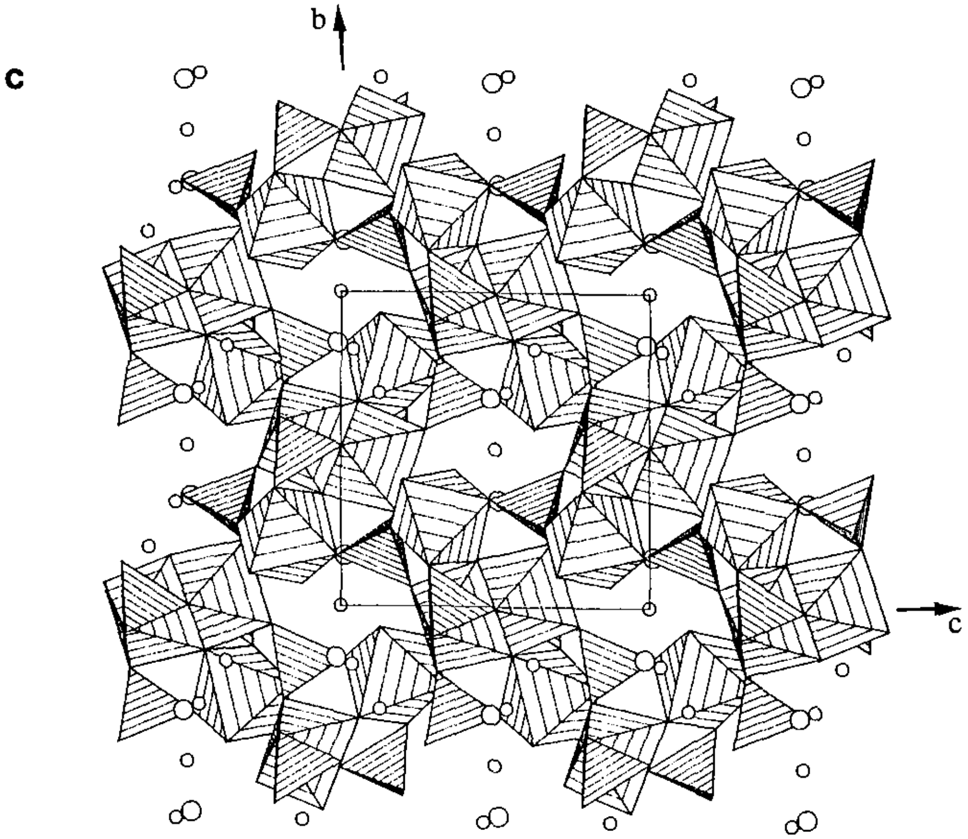

FIG. 1—*Continued*

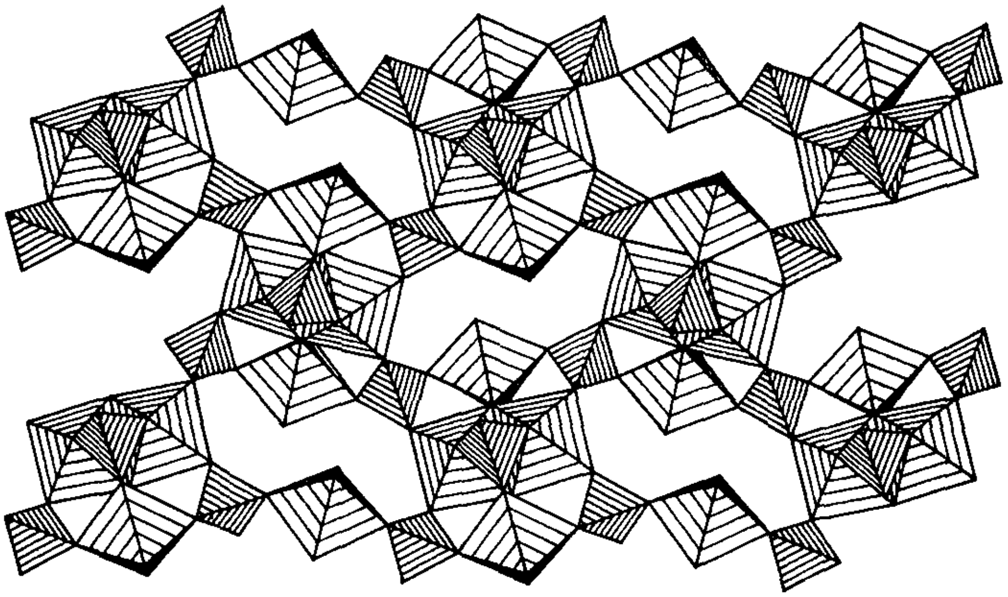

FIG. 2. Projection of the $RbMo_2P_2O_{10}\cdot 0.9H_2O$ structure along the perpendicular to (100).

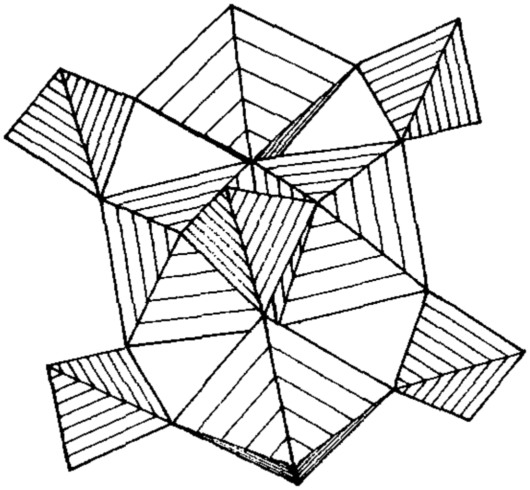

FIG. 3. The Mo_4O_{20} unit bridged with PO_4 tetrahedra.

CONCLUDING REMARKS

The synthesis of the monophosphate $RbMo_2P_2O_{10} \cdot 0.9H_2O$ demonstrates that the leucophosphite structure can be synthesized with conventional techniques, especially using normal pressures. The important characteristic of this microporous structure, which is evident here, deals with the possibility of occupancy of three kinds of sites by inserted cations or molecules. This feature, different from that observed from $NH_4Mo_2P_2O_{10} \cdot H_2O$, suggests that it should be possible to induce large deviations from stoichiometry on the interpolated cations, provided the Mo(V) specificity be conserved in order to ensure a great flexibility of the structure.

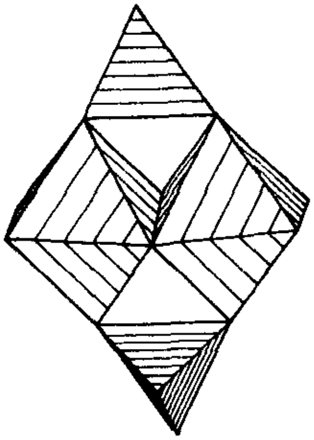

FIG. 4. $Mo_2P_2O_{14}$ unit.

TABLE 5

Main Distances (Å) and Angles (°) in the Polyhedra

Mo(1)	O(1)	O(2)	O(3)	O(4)	O(5)	O(6)
O(1)	1.654(9)	2.73(2)	2.73(2)	2.85(2)	2.78(2)	3.89(2)
O(2)	96.1(4)	2.008(8)	3.99(2)	2.86(2)	2.69(2)	2.88(2)
O(3)	95.6(4)	166.9(4)	2.017(8)	2.97(2)	2.81(2)	2.82(2)
O(4)	100.0(4)	89.7(3)	93.9(4)	2.050(8)	4.01(2)	2.77(2)
O(5)	98.1(4)	84.2(4)	88.5(4)	161.5(4)	2.011(9)	2.78(2)
O(6)	178.6(4)	85.2(3)	83.0(3)	80.5(3)	81.6(3)	2.234(9)

Mo(2)	O(4^{i})	O(4^{ii})	O(7)	O(8)	O(9)	O(10)
O(4^{i})	2.001(8)	3.16(2)	4.05(2)	2.77(2)	2.94(2)	2.80(2)
O(4^{ii})	104.5(3)	1.989(8)	2.75(2)	4.02(2)	2.74(2)	2.89(2)
O(7)	169.1(3)	85.6(3)	2.064(9)	2.74(2)	2.87(1)	2.80(2)
O(8)	86.4(3)	168.3(3)	83.8(4)	2.049(9)	2.82(2)	2.92(2)
O(9)	94.5(3)	86.7(3)	89.9(3)	88.1(4)	2.001(8)	4.01(2)
O(10)	88.5(3)	92.6(3)	87.1(3)	91.8(3)	177.0(3)	2.012(8)

P(1)	O(2)	O(3^{ii})	O(7)	O(8^{iii})
O(2)	1.532(9)	2.43(1)	2.55(1)	2.49(1)
O(3^{ii})	105.2(5)	1.532(9)	2.52(1)	2.51(1)
O(7)	112.9(5)	110.5(5)	1.533(9)	2.48(1)
O(8^{iii})	109.2(5)	110.6(5)	108.4(5)	1.520(9)

P(2)	O(5)	O(6^{iv})	O(9^{v})	O(10^{vi})
O(5)	1.514(9)	2.48(1)	2.47(1)	2.56(1)
O(6^{iv})	110.6(5)	1.505(9)	2.50(1)	2.53(1)
O(9^{v})	106.3(5)	109.4(5)	1.565(9)	2.52(1)
O(10^{vi})	112.6(5)	110.8(5)	107.0(5)	1.565(9)

Rb(1)–O(1^{vii}) = 3.389(9)
Rb(1)–O(2^{viii}) = 3.161(9)
Rb(1)–O(3) = 3.461(9)
Rb(1)–O(5^{viii}) = 3.345(9)
Rb(1)–O(5^{vii}) = 3.311(9)
Rb(1)–O(6) = 3.040(9)
Rb(1)–O(7^{vi}) = 2.960(9)
Rb(1)–O(8^{vii}) = 3.498(9)
Rb(1)–O(9^{vii}) = 2.902(9)
Rb(1)–O(10^{vi}) = 2.876(9)
Rb(1)–OH_2^{viii} = 2.941(12)

Rb(2)–O(2^{viii}) = 2.97(2)
Rb(2)–O(5^{viii}) = 3.13(2)
Rb(2)–O(6^{viii}) = 3.14(2)
Rb(2)–O(7^{vi}) = 2.94(2)
Rb(2)–O(8^{vi}) = 3.21(2)
Rb(2)–O(9^{vii}) = 3.27(2)
Rb(2)–O(10^{vi}) = 2.95(2)

Rb(3)–O(2^{iv}) = 3.002(9)
Rb(3)–O(2^{viii}) = 3.002(9)
Rb(3)–O(3^{ix}) = 2.893(9)
Rb(3)–O(3) = 2.893(9)
Rb(3)–O(10) = 2.943(8)
Rb(3)–O(10^{x}) = 2.943(8)
Rb(3)–OH_2^{iv} = 3.025(14)
Rb(3)–OH_2^{viii} = 3.025(14)
Rb(3)–O(6^{iv}) = 3.341(9)
Rb(3)–O(6^{viii}) = 3.341(9)
Rb(3)–O(8^{vi}) = 3.342(8)
Rb(3)–O(8^{x}) = 3.342(8)

Symmetry codes

i = $-x; -\frac{1}{2} + y; \frac{1}{2} - z$
ii = $x; \frac{1}{2} - y; \frac{1}{2} + z$
iii = $-x; \frac{1}{2} + y; \frac{1}{2} - z$
iv = $1 - x; -\frac{1}{2} + y; \frac{1}{2} - z$
v = $1 - x; y; 1 - z$
vi = $1 + x; -y; z$
vii = $1 - x; \frac{1}{2} + y; \frac{1}{2} - z$
viii = $x; \frac{1}{2} - y; -\frac{1}{2} + z$
ix = $1 - x; -y; -z$
x = $-x; -y; -z$

ACKNOWLEDGMENT

We thank Dr. Lamotte, in Lavalley's laboratory for collecting infrared spectra data.

REFERENCES

1. R. C. Haushalter, *J. Chem. Commun.* 1566 (1987).
2. A. Leclaire, M. M. Borel, A. Grandin, and B. Raveau, *Z. Kristallogr.* **184,** 247 (1988).
3. A. Leclaire, M. M. Borel, A. Grandin, and B. Raveau, *Eur. J. Solid State Inorg. Chem.* **26,** 45 (1989).
4. K. H. Lii, J. J. Chen, and S. L. Wang, *J. Solid State Chem.* **78,** 178 (1989).
5. K. H. Lii, R. C. Haushalter, and C. J. Connor, *Angew. Chem. Int. Ed. Eng.* **26,** 546 (1987).
6. K. H. Lii and C. C. Wang, *J. Solid State Chem.* **77,** 117 (1988).
7. R. C. Haushalter and F. W. Lai, *J. Solid State Chem.* **76,** 218 (1988).
8. A. Leclaire, M. M. Borel, A. Grandin, and B. Raveau, *J. Solid State Chem.* **78,** 220 (1989).
9. R. C. Haushalter, *J. Solid State Chem.* **89,** 215 (1990).
10. R. C. Haushalter, H. E. King, J. R., L. A. Mundi, and K. G. Strohmaier, *J. Solid State Chem.* **92,** 154 (1991).
11. H. E. King, J. R., L. A. Mundi, K. G. Strohmaier, and R. C. Haushalter, *J. Solid State Chem.* **92,** 1 (1991).
12. G. Costentin, M. M. Borel, A. Grandin, A. Leclaire, and B. Raveau, *J. Solid State Chem.* **95,** 168 (1991).
13. D. Riou and M. Goreaud, *J. Solid State Chem.* **79,** 99 (1989).
14. M. M. Borel, M. Goreaud, A. Grandin, Ph. Labbe, A. Leclaire, and B. Raveau, *Eur. J. Solid State Inorg. Chem.* **28,** 93 (1991).
15. I. D. Brown and A. Altermatt, *Acta Crystallogr. Sect. B* **41,** 244 (1985).